Journal of Sound and Vibration 330 (2011) 1141–1152

Contents lists available at ScienceDirect

Journal of Sound and Vibration

journal homepage: www.elsevier.com/locate/jsvi

Structural health monitoring of fixed offshore structures using the bicoherence function of ambient vibration measurements

A.J. Hillis [a,*], C.R.P. Courtney [b]

[a] University of Bath, Department of Mechanical Engineering, Bath BA2 7AY, UK
[b] University of Bristol, Department of Mechanical Engineering, Bristol BS8 1TR, UK

ARTICLE INFO

Article history:
Received 5 March 2010
Received in revised form
6 September 2010
Accepted 21 September 2010
Handling Editor: I. Trendafilova
Available online 13 October 2010

ABSTRACT

This paper investigates the use of the bicoherence function of measured structural acceleration to provide automatic early detection of damage in an offshore structure. A detailed simulation model is developed, including realistic wave loading, and is used to assess the performance of the method. The method is shown through analytical and numerical analysis to be insensitive to typical operating parameter variations and to variations in wave excitation force. It is demonstrated that very small changes in stiffness of individual structural members are detectable from measurements of global structural motion.

1. Introduction

Fatigue cracks are a common cause of failure in engineering structures. In many cases they cannot be eliminated so a Structural Health Monitoring (SHM) programme is essential for safe operation. Commonly this involves periodic inspection for fatigue damage using a measurement technique such as ultrasound, X-ray or eddy current. These techniques make local measurements, so the inspection of the whole structure is often extremely time-consuming, expensive, prone to human error and in many cases is not possible due to access limitations.

A global method for detecting damage in a structure is a desirable goal that has been pursued for many years, and a range of global non-destructive testing (NDT) techniques have been developed. Worden et al. [1] used neural networks to diagnose a fault in a component based on analysis of its low-frequency nonlinear dynamic response. Solodov [2], Kazakov et al. [3] and Morbidini et al. [4] suggested the use of the vibroacoustic modulation technique, in which the low-frequency resonance of a structure is used to open and close a crack. The crack is then probed by a high-frequency (typically ultrasonic) signal, and the low-frequency vibration modulates the ultrasonic probing pulses producing energy at the sum and difference frequencies. Other methods include, for example, detecting changes in natural frequencies and mode shapes [5–7], modeshape curvature [8] and flexibility [9]. While they have found some application areas, these methods suffer from various limitations. Often, the sensitivity to small defects is not sufficient for most applications and the approaches are inherently sensitive to geometry and boundary condition changes. For fixed offshore structures, significant changes in these parameters can be caused by factors other than damage, such as typical operating variations in topside mass, mass distribution and pile conditions.

There is a body of evidence showing that a range of common defects, including fatigue cracking, exhibit dynamic nonlinear responses over a range of frequencies, and that these nonlinear effects can be used for detecting damage [10,11]. If the crack is

* Corresponding author. Tel.: +44 1225384977.
E-mail address: a.j.hillis@bath.ac.uk (A.J. Hillis).

0022-460X/$ - see front matter © 2010 Elsevier Ltd. All rights reserved.
doi:10.1016/j.jsv.2010.09.019

activated then the cracked member will have a different stiffness depending on whether it is open or closed. In this study a global damage detection strategy is developed that capitalizes on the nonlinear effects introduced by fatigue damage. This strategy is based upon higher order spectral analysis (HOSA), more specifically bicoherence analysis, which has received significant attention in recent years in many applications. These include detection of loose bolted joints [12], fatigue cracks in beams [11], bearing defects [13] and weak structural nonlinearities [14]. The bispectrum (a subset of HOSA, and related to bicoherence) has been used in conjunction with neural networks in order to characterize different types of structural defects [15–17]. The bicoherence of a signal has been shown to detect nonlinear components resulting from bilinear system responses. For structural applications, as described here, this could include the effects of geometric nonlinearity as well as fatigue damage. Therefore, a baseline case should be used as a means for comparison and determining the increase in damage. This baseline case could be the intact structure or, if this is not available, a finite element (FE) model. Certain other types of damage will not exhibit a bilinear effect and will therefore not be detected by the bicoherence technique (e.g. corrosion will result in reduced stiffness, but not in a bilinear sense since the reduced stiffness would be apparent for both compression and tension in the damaged member).

The aforementioned studies have investigated the use of the bicoherence technique in the detection of damage in simple structures. It is interesting to study whether the technique can be used to detect relatively small levels of damage in large structures. The application of offshore structures is highly relevant due to the emphasis on safety within the industry, the value to the global economy, and the large number of ageing platforms and newer platforms built in more extreme environments. In this study, the bicoherence method is used to detect the effects of simulated fatigue damage in a single (highly utilized) member of a fixed offshore platform model using measurements of ambient vibration. The model and loading are described in detail in Sections 2 and 3, and the bicoherence method is described in Section 4. Insensitivity to nonlinear effects from wave loading are demonstrated analytically, and it is shown through simulation that small changes in stiffness of a single member can be detected from measurements of global vibration. Furthermore it is demonstrated that the detection of damage is not sensitive to normal variations in mass, system damping or seastate excitation.

2. Structural dynamics

In this study a typical unmanned platform in the Southern North Sea is considered as an example. The support structure has a height of 55 m, sits in water with depth 40 m and supports a mass M_1 = 500 Tonne. The structure is shown in Fig. 1.

The platform structure was discretized to approximately 2000 degrees of freedom (DOF) representing nodal displacements and rotations. The undamped dynamic response of the system is described by the multi-DOF equation of motion:

$$\mathbf{M}\ddot{\boldsymbol{q}} + \mathbf{K}\boldsymbol{q} = \boldsymbol{f} \tag{1}$$

where $\boldsymbol{q}$ is the vector of nodal displacements and rotations, $\boldsymbol{f}$ is the vector of external forces associated with the degrees of freedom, and $\mathbf{M}$ and $\mathbf{K}$ are the mass and stiffness matrices obtained from the FE model. A model of this size is computationally inefficient and contains information on many higher modes which are uncertain and not significant, since they have small modal participation factors. It is sensible, therefore, to produce a reduced-order model for subsequent analysis. Here the approach of Tilley et al. [18] is adopted. The modal matrix equation for the free undamped system may be written as

$$\mathbf{M}\mathbf{Q}\boldsymbol{\Lambda} = \mathbf{K}\mathbf{Q} \tag{2}$$

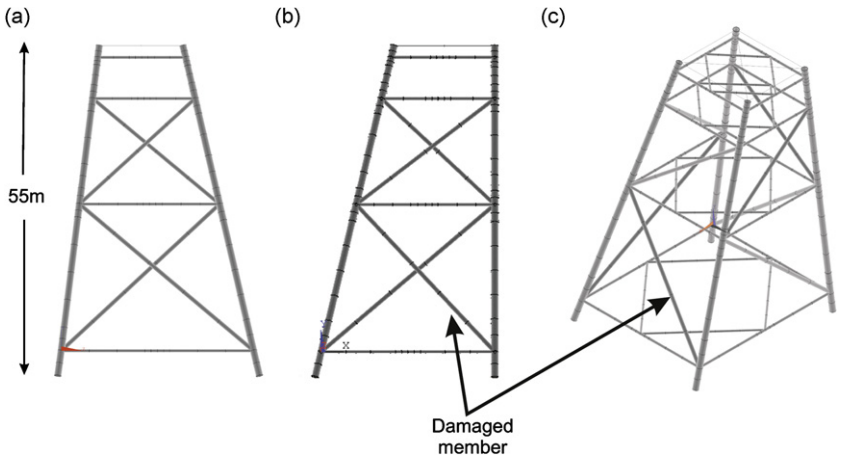

Fig. 1. Supporting structure model in ANSYS. (a) Front view. (b) Side view. (c) Isometric view.

where $\mathbf{Q}=[\boldsymbol{q}_1\cdots\boldsymbol{q}_N]$ is the matrix of eigenvectors, and $\boldsymbol{\Lambda}=\mathrm{diag}[\omega_1^2,\ldots,\omega_2^2]$ is the matrix of eigenvalues. The modal mass and stiffness matrices are defined as

$$\mathbf{Q}^{\mathrm{T}}\mathbf{M}\mathbf{Q}=\mathrm{diag}[m_1,\ldots,m_N]$$

$$\mathbf{Q}^{\mathrm{T}}\mathbf{K}\mathbf{Q}=\mathrm{diag}[k_1,\ldots,k_N]=\mathbf{Q}^{\mathrm{T}}\mathbf{M}\mathbf{Q}\boldsymbol{\Lambda} \tag{3}$$

The modal matrices are ordered with increasing ω_i and the lowest 6 modes extracted to capture only the significant structural dynamics. The first three modes (translation in x- and y-directions and torsion about z) and their corresponding natural frequencies are shown in Fig. 2.

Nodal displacements and rotations may be expressed as the combination of mode shape vectors:

$$\boldsymbol{q}=\rho_1\boldsymbol{q}_1+\cdots+\rho_N\boldsymbol{q}_N=\mathbf{Q}\boldsymbol{\rho} \tag{4}$$

where $\boldsymbol{\rho}=[\rho_1\cdots\rho_N]^{\mathrm{T}}$ is the modal coordinate vector. Substituting Eq. (4) into Eq. (1), and using the definitions for modal mass and stiffness matrices (Eq. (3)), the system can be described by

$$\ddot{\boldsymbol{\rho}}+\boldsymbol{\Lambda}\boldsymbol{\rho}=(\mathbf{Q}^{\mathrm{T}}\mathbf{M}\mathbf{Q})^{-1}\mathbf{Q}^{\mathrm{T}}\boldsymbol{f}=\mathbf{B}\boldsymbol{f} \tag{5}$$

where $\mathbf{B}$ maps the forces to modal coordinates. The matrices may now be sorted in ascending order of the natural frequency terms in $\boldsymbol{\Lambda}$, allowing Eq. (4) to be partitioned into low- and high-frequency components:

$$\begin{bmatrix}\ddot{\boldsymbol{\rho}}_L\\ \ddot{\boldsymbol{\rho}}_H\end{bmatrix}+\begin{bmatrix}\boldsymbol{\Lambda}_L & \mathbf{0}\\ \mathbf{0} & \boldsymbol{\Lambda}_H\end{bmatrix}\begin{bmatrix}\boldsymbol{\rho}_L\\ \boldsymbol{\rho}_H\end{bmatrix}=\begin{bmatrix}\mathbf{B}_L\\ \mathbf{B}_H\end{bmatrix}\mathbf{f} \tag{6}$$

The high-frequency modes are not significant and are therefore neglected. The significant low-frequency motion is obtained from

$$\ddot{\boldsymbol{\rho}}_L+\boldsymbol{\Lambda}_L\boldsymbol{\rho}_L=\mathbf{B}_L\boldsymbol{f} \tag{7}$$

Though the high-frequency modes are neglected, it is still necessary to include the static component of these modes to maintain accuracy. From Eq. (6) and ignoring the acceleration term, the static components of the high-frequency modes are given by

$$\boldsymbol{\rho}_{H0}=\boldsymbol{\Lambda}_H^{-1}\mathbf{B}_H\boldsymbol{f} \tag{8}$$

Including damping, Eq. (7) becomes

$$\ddot{\boldsymbol{\rho}}_L+\mathbf{B}_L\boldsymbol{\zeta}\dot{\boldsymbol{\rho}}_L+\boldsymbol{\Lambda}_L\boldsymbol{\rho}_L=\mathbf{B}_L\boldsymbol{f} \tag{9}$$

where $\boldsymbol{\zeta}=\mathrm{diag}[\zeta_1,\ldots,\zeta_L]$ is the damping matrix and, in this case, ζ_i is set to 2 percent of critical damping, or 0.02. The physical DOFs may now be obtained from

$$\boldsymbol{q}=\mathbf{Q}_L\boldsymbol{\rho}_L+\mathbf{Q}_H\boldsymbol{\rho}_{H0} \tag{10}$$

Damage can be introduced by reducing the stiffness of individual members in the structure and repeating this process with the resulting new mass and stiffness matrices. A bilinear system can be achieved by switching between nominal and damaged system models depending upon the relative motion of the ends of the damaged member (i.e. whether a fatigue

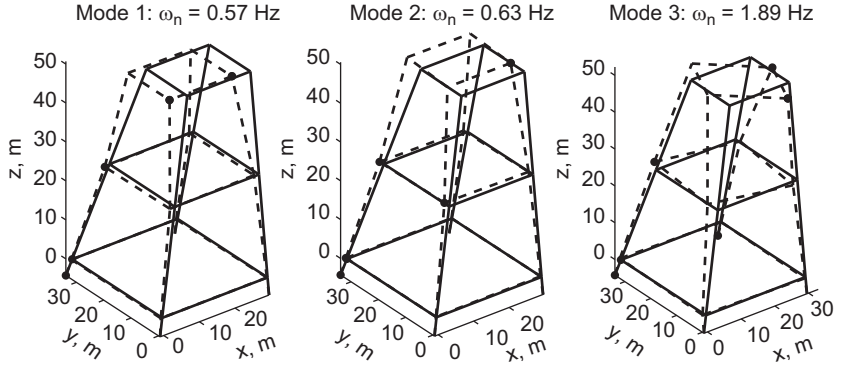

Fig. 2. First three structural vibration modes and natural frequencies. Dashed lines are deflected shapes. Diagonal members omitted for clarity.

crack would be open or closed). This system was implemented as a time-domain simulation in SIMULINK and used to obtain the motion of several points on the structure. The details of the wave loads applied are discussed in the following section.

3. Wave loading

Irregular ocean waves contain a spectrum of frequencies $S(\omega)$. For the purposes of this investigation the example of a platform located in the North Sea is used. The appropriate spectrum for the North Sea is the JONSWAP spectrum [19], which is given by

$$S(\omega) = \left(\frac{5H_s}{16\omega_p}\right)\left(\frac{\omega_p}{\omega}\right)^5 \exp\left[-1.25\left(\frac{\omega}{\omega_p}\right)^{-4}\right]\gamma^\beta \tag{11}$$

where H_s is the significant wave height, ω_p is the peak angular frequency ($\omega = 2\pi f$ if f is the frequency in Hz), γ^β is a frequency-dependent factor that controls the sharpness of the peak, and β is given by

$$\beta = \exp\left(\frac{-(\omega-\omega_p)^2}{2\tau^2\omega_p^2}\right) \tag{12}$$

where τ takes the values $\tau = 0.07$ ($\omega \le \omega_p$), $\tau = 0.09$ ($\omega > \omega_p$). In this investigation, two seastates are used. Seastate 1 takes the values H_s=4 m, f_p=0.14 Hz, $\gamma = 3.3$ and Seastate 2 takes the values H_s=7 m, f_p=0.10 Hz and $\gamma = 3.3$. These represent typical analysis conditions for the North Sea. The resulting JONSWAP spectra and wave force power spectral densities (PSD) are shown in Fig. 3.

For a structure in unidirectional waves, $\boldsymbol{f}'(z,t)$ is the wave force per unit length at a height z above the seabed and is calculated from Morison's equation [20]

$$\boldsymbol{f}'(z,t) = \frac{1}{2}\rho C_D D|\dot{\mathbf{x}}_w - \dot{\boldsymbol{x}}_s|(\dot{\boldsymbol{x}}_w - \dot{\boldsymbol{x}}_s) + \rho C_I \frac{\pi D^2}{4}\ddot{\boldsymbol{x}}_w - \rho(C_I - 1)\frac{\pi D^2}{4}\ddot{\boldsymbol{x}}_s \tag{13}$$

where $\mathbf{x}_s(z,t)$ and $\mathbf{x}_w(z,t)$ are the horizontal displacement of the structure and the wave particle, respectively, D is the diameter of the structural members, ρ is the density of sea water and C_D and C_I are drag and inertia coefficients (which typically take values of 1 and 2, respectively [21]).

From linear wave theory, the horizontal wave particle velocity $\dot{\mathbf{x}}_w(z,t)$ at depth z is given by the expression

$$\dot{\boldsymbol{x}}_w(z,t) = \sum_{i=1}^{N} \frac{\omega_i \cosh(k_i z)}{\sinh(k_i d)}\sqrt{\frac{S(\omega_i)}{\omega_i}}\cos(\omega_i t + \phi_i) \tag{14}$$

where d is the water depth, k_i and ϕ_i are the wavenumber the random phase of the ith frequency component in the length N discretized wave spectrum. For deep water the approximation $k = \omega^2/g$ is valid.

A realistic horizontal wave particle velocity vector may be obtained by filtering a white noise signal with a bank of finite impulse response (FIR) filters (one entry for each depth coordinate z) designed to approximate the frequency characteristics of Eq. (14) [22]. From this $\boldsymbol{f}'(z,t)$ may be calculated for submerged nodes on the structure, and multiplying by the equivalent member length for each node yields the required force input vector $\boldsymbol{f}$.

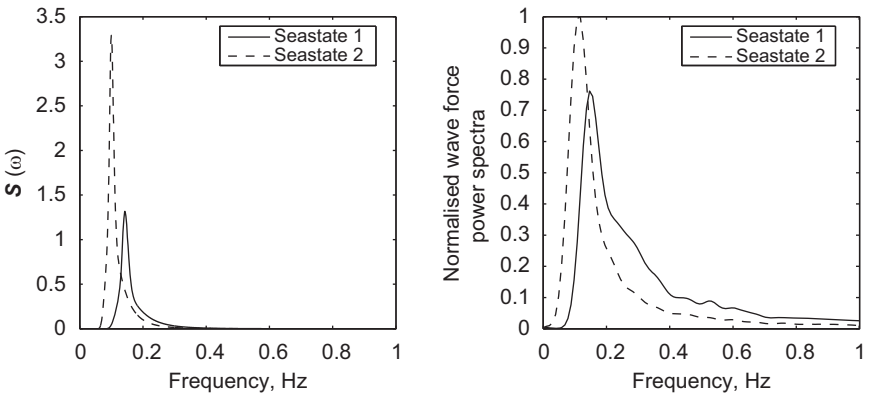

Fig. 3. JONSWAP spectra and wave force PSDs for typical North Sea conditions.

4. Bispectral/bicoherence analysis for damage detection

4.1. The bispectrum and the bicoherence function

The bicoherence is a normalized form of the bispectrum, which is a third-order spectrum that has attracted substantial interest in the analysis of signals from systems that exhibit nonlinearity.

A signal $y(t)$ whose Fourier transform is

$$Y(f) = \int_{t=-\infty}^{\infty} y(t)\exp[2\pi jft]\,\mathrm{d}t \tag{15}$$

has a power spectrum

$$P(f) = \mathrm{E}[Y(f)Y^*(f)] \tag{16}$$

where * indicates the complex conjugate and E[⋯] denotes the expectation value operator (or average over a statistical ensemble). The direct definition of the bispectrum of the signal $y(t)$ is [23,24]

$$\mathrm{B}(f_1,f_2) = \mathrm{E}[Y(f_1)Y(f_2)Y^*(f_1+f_2)] \tag{17}$$

From Eq. (17) it can be seen that, while the power spectrum involves the spectral component at only one frequency, the bispectrum depends on the components at three frequencies: f_1, f_2 and f_1+f_2. This leads to the bispectrum providing information about the coupling between frequencies and hence has useful properties when considering nonlinear systems. More precisely, the bispectrum will be non-zero only if the amplitude at frequency components f_1, f_2 and f_1+f_2 are non-zero and the phases of those components obey the rule $\phi_3 = \phi_1 + \phi_2$ [23]. This relationship is known as quadratic phase coupling (QPC) and is associated with quadratic nonlinearity. For stochastic processes, the bispectrum is zero for Gaussian series and Gaussian series that have been subjected to a linear process [25]. For weakly nonlinear, non-Gaussian processes, the bispectrum gives a measure of the QPC and hence of the level of quadratic nonlinearity in the process [26].

The bispectrum is not normalized with regard to signal amplitude and so includes information on the magnitude of the signals involved as well as the degree of coupling between them. In order to isolate information on the degree of coupling, Kim and Powers defined the bicoherence as [23]

$$\mathrm{b}(f_1,f_2) = \frac{|\mathrm{B}(f_1,f_2)|}{\sqrt{\mathrm{E}[|Y(f_1)Y(f_2)|^2]\mathrm{E}[|Y(f_1+f_2)|^2]}} \tag{18}$$

This was developed to have the useful property that it is bounded by zero and one ($0 \le \mathrm{b}(f_1,f_2) \le 1$) and that (for three-wave coupling) it gives the fraction of signal energy that is due to quadratic coupling [23]. The interpretation in the case of broadband stochastic signals is less clear [27,28], but Herbers and Guza argued that the bicoherence can be interpreted as a lower bound on the energy at f_1+f_2 that is nonlinearly coupled to energy at f_1 and f_2 [29,30].

4.2. Estimation of bicoherence

The evaluation of the bicoherence function requires the evaluation of three expectation values of products of signals in the frequency domain. In practice (and in this work) this is achieved by dividing data into a number of records M of length N, performing the discrete Fourier transform on each, multiplying the appropriate terms and then averaging over the M records. Each record may be zero padded and the discrete Fourier transform performed for an effective signal length $N_{\mathrm{DFT}} > N$. Broadly speaking:

- increasing the number of records M decreases the variance of the estimate;
- increasing the number of data points per record N decreases the variance and increases the frequency resolution;
- increasing the Fourier transform length N_{DFT} interpolates in the frequency domain to clarify the spectrum.

Consider a discrete record $y_i(t_k)$ measured at times $t_k = k\Delta t$, where k=0,1,2,…,$(N-1)$ and $\Delta t = 1/f_s$. There are M, potentially overlapping, records labelled i, where i=1,2,…,M. For each record the frequency content is obtained by the discrete Fourier transform

$$\hat{Y}_i(f_n) = \frac{1}{N}\sum_{k=0}^{N-1} y_i(t_k)\exp(-\mathrm{j}2\pi nk/N_{\mathrm{DFT}}) \tag{19}$$

assessed at $f_n = n/(N_{\mathrm{DFT}}\Delta t)$ and n=0…$N_{\mathrm{DFT}}-1$. Using averages over M records to approximate the expectation values the bispectrum, defined in Eq. (17), is obtained as

$$\hat{B}(f_1,f_2) = \frac{1}{M}\sum_{i=1}^{M}[\hat{Y}_i(f_1)\hat{Y}_i(f_2)\hat{Y}_i^*(f_1+f_2)] \tag{20}$$

Similarly the bicoherence (Eq. (18)) is approximated as

$$\hat{b}(f_1,f_2)=\frac{|\hat{B}(f_1,f_2)|}{\frac{1}{M}\sum_{i=1}^{M}(|\hat{Y}_i(f_1)\hat{Y}_i(f_2)|^2)\frac{1}{M}\sum_{i=1}^{M}(|\hat{Y}_i(f_1+f_2)|^2)} \tag{21}$$

It should be noted that there have been some criticisms of the Kim and Powers definition of the bicoherence. The most serious (practically speaking) is that increasing the length of the record used to estimate the bicoherence changes the measured value. Specifically, for long datasets the bicoherence tends to zero [31] and so care needs to be taken in selecting the parameters used in the estimate (a parameter sensitivity study is provided in Section 6.2).

5. Motivation for application of bicoherence to fixed offshore structures

The bispectrum and bicoherence have both attracted interest in a wide variety of systems where nonlinear behaviour is of interest. Possible sources of nonlinearity in the system considered in this work include:

1. Structural stiffness variations due to fatigue damage.
2. Normal operating variations to the structure, including changes in mass (e.g. equipment/fluid loading and offloading), stiffness (e.g. pile/soil conditions) and damping (e.g. marine growth and wave excitation variations).
3. Nonlinear wave excitation due to nonlinearity in the wave forms and due to the nonlinear drag term in the wave force equation (Eq. (13)).

Ideally a damage detection process would be sensitive only to structural stiffness variations due to damage. For the bicoherence method described here, sensitivity to fatigue damage and insensitivity to nonlinear drag are demonstrated analytically in this section by considering two model systems:

1. a bilinear spring, representing a partially fatigued member;
2. a linear spring acting against a viscous drag force, representing the coupling of the sea waves to the structure.

These models are intentionally simplistic and serve to demonstrate analytically the ability of the bicoherence technique to detect bilinear system responses while being insensitive to nonlinear responses due to wave–structure interaction. More detailed simulation studies in Section 6 support this analysis and demonstrate the insensitivity to normal operating variations and seastates (excitation spectra).

A simple sinusoidal excitation is sufficient to demonstrate the nonlinear response of each system and allows an analytical solution to be determined and easily interpreted. Excitation by a sinusoidal signal $x(t)$ of frequency f_1, amplitude A_1 and phase ϕ_1,

$$x(t)=A_1\sin(2\pi f_1 t+\phi_1) \tag{22}$$

generates a response $y(t)$ of the system which is a function of only the input, i.e.

$$y(t)=f\{x(t)\} \tag{23}$$

Interest in the bicoherence stems from its ability to determine how much of a signal is related to quadratic coupling. To demonstrate this a second signal, at the harmonic frequency $2f_1$, is added to the response signal when demonstrating the bicoherence behaviour, such that the system response is given by

$$y'(t)=y(t)+A_2\sin(4\pi f_1 t+\phi_2) \tag{24}$$

As with the input $x(t)$, the amplitude, A_2, and phase, ϕ_2, of $y'(t)$, are randomly distributed. Ideally the bispectrum should be a function of the nonlinear signal generated by the system, and not of the additional signal which is not quadratically phase coupled. In the wave-driven system this property allows the nonlinear signal to be distinguished from the linear response to the broadband excitation.

5.1. Bilinear spring—a simplified model for a structure with fatigue damage

Consider the case of a bilinear system (a simple model of a partially damaged structure) which is stiffer in compression than in tension. The response (force) resulting from the application of displacement $x(t)$ can be written as

$$y(t)=K(x(t))x(t) \tag{25}$$

where the stiffness is given by

$$K(x(t))=\begin{cases}(K-\Delta K)x(t), & y(t)>0\\ Kx(t), & y(t)\le 0\end{cases} \tag{26}$$

Using the excitation defined in Eq. (22) the response can be written as

$$y(t) = Kx(t) - \Delta K[\Delta_T(t-t_\Delta) * \Pi_{T/2}(t)]x(t) \tag{27}$$

where * indicates convolution. Two new functions are introduced: the Dirac Comb, $\Delta_T(t)$, and the top hat function, $\Pi_W(t)$, which are defined by

$$\Delta_T(t) = \sum_{n=-\infty}^{\infty} \delta(t-nT) \tag{28}$$

$$\Pi_W(t) = \begin{cases} 0, & t < -\dfrac{W}{2} \\ 1, & -\dfrac{W}{2} \le t \le \dfrac{W}{2} \\ 0, & t > \dfrac{W}{2} \end{cases} \tag{29}$$

where W is the width of the top hat function.

The convolution $\Delta_T(t-t_\Delta) * \Pi_{T/2}(t)$ gives a train of top hat functions of width $T/2$ with a period of $T=1/f_1$. The parameter t_Δ is defined to give the centre of each top hat coincident with the first maximum of the excitation. Evaluating the Fourier transform gives

$$Y(f) = \frac{jKA_1}{2}(\delta(f+f_1)e^{-j\phi_1} - \delta(f-f_1)e^{j\phi_1}) + \frac{j\Delta KA_1}{4}\Delta_F(f)\left\{\operatorname{sinc}\left(\frac{\pi(f+f_1)T}{2}\right)e^{-j2\pi(f+f_1)t_\Delta}e^{-j\phi_1} - \operatorname{sinc}\left(\frac{\pi(f-f_1)T}{2}\right)e^{-j2\pi(f-f_1)t_\Delta}e^{j\phi_1}\right\}. \tag{30}$$

where $\operatorname{sinc} x = \sin(x)/x$.

At the excitation frequency f_1 this gives

$$Y(f_1) = -\frac{jA_1}{2}\left(Ke^{-j\phi_1} + \frac{\Delta K}{2}e^{j\phi_1}\right) \tag{31}$$

and for the harmonic $2f_1$

$$Y(2f_1) = \frac{\Delta KA_1}{4j}\left\{\operatorname{sinc}\left(\frac{\pi}{2}\right)e^{-j\pi/2} - \operatorname{sinc}\left(\frac{3\pi}{2}\right)e^{-j3\pi/2}\right\}e^{2j\phi_1} = \frac{\Delta KA}{3\pi}e^{2j\phi_1} \tag{32}$$

If the system is weakly nonlinear, i.e. $K \gg \Delta K$, then the second term of Eq. (31) can be neglected. This allows the bispectrum at f_1, f_1 to be written as

$$B(f_1,f_1) = E[Y(f_1)Y(f_1)Y^*(f_1)] = E\left[\left(-\frac{jKA_1}{2}e^{j\phi_1}\right)\left(-\frac{jKA_2}{2}e^{j\phi_1}\right)\frac{\Delta KA_1}{3\pi}e^{-2j\phi_1}\right] = -\frac{K^2\Delta K}{12\pi}E[A_1^3] \tag{33}$$

This indicates that the bispectrum can be used to detect the response of a bilinear system.

In order to assess the ability to distinguish a signal at $2f_1$ due to nonlinearity and an uncorrelated signal consider the frequency content of the output given in Eq. (24), which adds an uncorrelated signal at $2f_1$ to the response

$$Y'(f) = Y(f) + j\frac{A_2}{2}(\delta(f+2f_1)e^{-j\phi_2} - \delta(f-2f_1)e^{j\phi_2}) \tag{34}$$

The bispectrum of the combined signal at (f_1,f_1) can be written as

$$B_m(f_1,f_1) = B(f_1,f_1) + E\left[\left(-\frac{jKA_1}{2}e^{j\phi_1}\right)\left(-\frac{jKA_1}{2}e^{j\phi_1}\right)j\frac{A_2}{2}e^{-j\phi_2}\right] = B(f_1,f_1) + jK^2E[A_1^2A_2e^{j(2\phi_1-\phi_2)}] = B(f_1,f_1) + jK^2E[A_1^2][A_2][e^{j(2\phi_1-\phi_2)}] = B(f_1,f_1) \tag{35}$$

This results from the uncorrelated random distribution of phases ϕ_1 and ϕ_2 resulting in an expectation value of the exponential term $e^{j(2\phi_1-\phi_2)}$ equal to zero. Hence, for this sample system the bispectrum discounts the uncorrelated signal and only measures the signal due to nonlinearity.

In order to calculate the bicoherence two other values are needed:

$$E[|Y'(f_1)Y'(f_1)|^2] = E\left[\left(-\frac{jKA_1}{2}e^{j\phi_1}\right)\left(-\frac{jKA_1}{2}e^{j\phi_1}\right)\left(\frac{jKA_1}{2}e^{-j\phi_1}\right)\left(\frac{jKA_1}{2}e^{-j\phi_1}\right)\right] = \frac{K^4}{16}E[A_1^4] \tag{36}$$

and

$$E[Y'(2f_1)Y'^*(2f_1)] = E\left[\left(\frac{\Delta KA_1}{3\pi}e^{2j\phi_1} - j\frac{A_2}{2}e^{j\phi_2}\right)\left(\frac{\Delta KA_1}{3\pi}e^{-2j\phi_1} + j\frac{A_2}{2}e^{-j\phi_2}\right)\right] = \frac{\Delta K^2}{9\pi}E[A^2] + \frac{1}{4}E[A_2^2] \tag{37}$$

substituting Eqs. (35)–(37) into the Kim and Powers definition of the bicoherence (Eq. (18)) gives

$$|\mathrm{b}(f_1,f_1)|^2 = \frac{\Delta K^2(\mathrm{E}[A_1^3])^2}{\Delta K^2\mathrm{E}[A_1^4]\mathrm{E}[A_1^2]+\frac{9\pi}{4}\mathrm{E}[A_1^4]\mathrm{E}[A_2^2]} \tag{38}$$

The bicoherence tends to zero where there is no nonlinearity ($\Delta K = 0$), and tends to unity if there is nonlinearity, but there is no uncorrelated signal at $2f_1$, $\mathrm{E}[A_2^2]=0$. This indicates that this measure has potential as a detector of bilinearity.

5.2. A model for nonlinear drag forces

Early interest in bispectral analysis was generated by work on its application to ocean wave signals. Nonlinearity of ocean wave records has been detected using the bispectrum [26,32,33], however these studies have concentrated on waves in shallow water, as internal waves in deep water do not produce significant bispectrum values in either wave height or wave power [27]. Fixed offshore platforms are located in deep water, where nonlinearity in the waves themselves can be neglected. It therefore remains to demonstrate the insensitivity of the bicoherence function to the nonlinear drag force in Eq. (13).

Consider the second sample system consisting of a linear spring along with a viscous drag term, with output

$$y(t) = Kx(t) - c\dot{x}(t)|\dot{x}(t)| \tag{39}$$

If the excitation $x(t)$ is as defined in Eq. (22) then the magnitude of $\dot{x}(t) = (\mathrm{d}/\mathrm{d}t)\sin(2\pi f_1 t+\phi_1) = 2\pi f_1\cos(2\pi f_1 t+\phi_1)$ can be written as

$$|\dot{x}(t)| = \mathrm{sgn}[\dot{x}(t)]\dot{x}(t) = \mathrm{sgn}(\cos(2\pi f_1 t+\phi_1))\dot{x} = (1-2\Delta_T(t-t_\Delta') * \Pi_{T/2}(t))\dot{x}(t) \tag{40}$$

where $\mathrm{sgn}[x]$ gives the sign of x and t_Δ' ensures that the repeated top hat function coincides with the minima (i.e. centre of the negative part) of the cosine.

The Fourier transform of $\dot{x}(t)$ is $j2\pi X(f)$, so the magnitude of the excitation may be written in the frequency domain as

$$\begin{aligned}\mathcal{F}[|\dot{x}(t)|] &= 2\pi jf\mathrm{X}(f) - 2\mathcal{F}[\Delta_T(t-t_\Delta')]\mathcal{F}[\Pi_{T/2}(t)] * 2\pi jf\mathrm{X}(f)\\ &= \pi f\{\delta(f_1+f)\mathrm{e}^{-j\phi_1} - \delta(f-f_1)\mathrm{e}^{j\phi_1}\} + \pi f_1\left\{\Delta_{f_1}(f-f_1)\mathrm{e}^{-j2\pi(f-f_1)t_\Delta'}\mathrm{sinc}\left(\frac{\pi(f-f_1)}{2f_1}\right)\mathrm{e}^{j\phi_1}\right\}\\ &\quad -\pi f_1\left\{\Delta_{f_1}(f+f_1)\mathrm{e}^{-j2\pi(f+f_1)t_\Delta'}\mathrm{sinc}\left(\frac{\pi(f+f_1)}{2f_1}\right)\mathrm{e}^{-j\phi_1}\right\}\end{aligned} \tag{41}$$

Denoting $C(f) = \mathcal{F}[|\dot{x}(t)|]$, then

$$\begin{aligned}\mathcal{F}[\dot{x}(t)|\dot{x}(t)|] &= 2j\pi f\mathrm{X}(f) * C(f) = -\pi f\{\delta(f_1+f)\mathrm{e}^{-j\phi_1} - \delta(f-f_1)\mathrm{e}^{j\phi_1}\} * C(f) = \pi f\delta(f-f_1)\mathrm{e}^{j\phi_1} * C(f) - \pi f\delta(f_1+f)\mathrm{e}^{-j\phi_1} * C(f)\\ &= \pi f_1 C(f-f_1)\mathrm{e}^{j\phi_1} + \pi f_1 C(f+f_1)\mathrm{e}^{-j\phi_1}\end{aligned} \tag{42}$$

and so

$$Y(f) = \frac{jKA_1}{2}(\delta(f+f_1)\mathrm{e}^{-j\phi_1} - \delta(f-f_1)\mathrm{e}^{j\phi_1}) + c\pi f_1 C(f-f_1)\mathrm{e}^{j\phi_1} + c\pi f_1 C(f+f_1)\mathrm{e}^{-j\phi_1} \tag{43}$$

Of interest for the calculation of $\mathrm{B}(f_1,f_1)$ is the response at the harmonic frequency $f=2f_1$, given by

$$Y(2f_1) = c\pi f_1 C(f_1)\mathrm{e}^{j\phi_1} + c\pi f_1 C(3f_1)\mathrm{e}^{-j\phi_1}. \tag{44}$$

Using Eq. (41) to evaluate $C(f)$ at the two frequencies of interest,

$$C(f_1) = \pi f_1\{0-\mathrm{e}^{j\phi_1}\} + \pi f_1\{\mathrm{sinc}(0)\mathrm{e}^{j\phi_1}\} - \pi f_1\mathrm{e}^{-j2\pi(2f_1)t_\Delta'}\mathrm{sinc}(\pi)\mathrm{e}^{-j\phi_1} = -\pi f_1\mathrm{e}^{j\phi_1} + \pi f_1\mathrm{e}^{j\phi_1} = 0 \tag{45}$$

$$C(3f_1) = \pi f\{0-0\} + \pi f_1\{\mathrm{e}^{-j2\pi(2f_1)t_\Delta'}\mathrm{sinc}(\pi)\mathrm{e}^{j\phi_1}\} - \pi f_1\{\mathrm{e}^{-j2\pi(4f_1)t_\Delta'}\mathrm{sinc}(2\pi)\mathrm{e}^{-j\phi_1}\} = 0 \tag{46}$$

Hence the signal at $2f_1$,

$$Y(2f_1) = 0 \tag{47}$$

This result indicates that the bispectrum (and hence the bicoherence) does not detect the nonlinearity due to viscous drag in the wave force applied to the structure.

6. Results

6.1. General results

Fig. 4 shows the bicoherence plots for acceleration response signals measured from a node at the top deck of the structure. For all results, Gaussian measurement noise was added at a level 40 dB down from signal level. Unidirectional waves generated from Seastate 1 were applied in the x-direction to the structure with three damage states, with the most highly stressed individual member being fatigued (simulated by reducing its stiffness). The damaged member is a lower diagonal and is marked in Fig. 1. The plots show results for the structure with this member intact, 50 percent through-

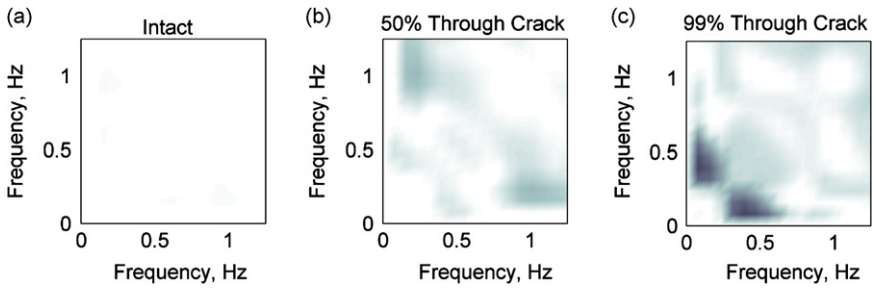

Fig. 4. Bicoherence plots of measured acceleration response at the top of the structure with three damage states.

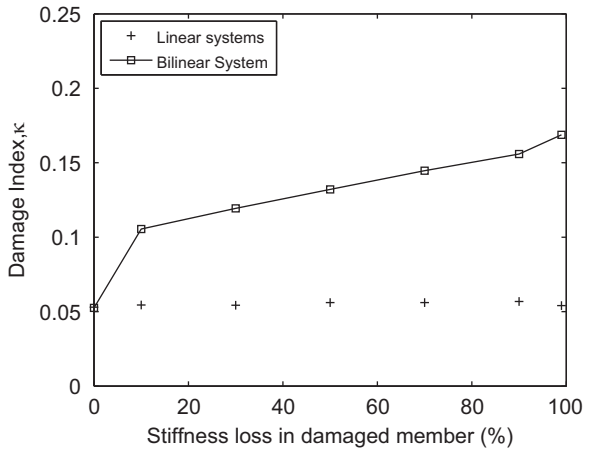

Fig. 5. Damage index for nominal system with different damage states (single member reduced stiffness). Results for bilinear and linear reduced stiffness models shown.

cracked, and 99 percent through-cracked as bilinear systems. Darker areas on these plots indicate greater nonlinear content in the response signal, so it is clear that increased damage has resulted in increased bicoherence values.

The bicoherence was averaged over the frequency range $0.05 < (f_i, f_j) < 2.50$ Hz to give a damage index:

$$\kappa = \frac{1}{N_f^2} \sum_{i=1}^{N_f} \sum_{j=1}^{N_f} \mathrm{b}(f_i, f_j) \tag{48}$$

N_f is the number of discrete frequency values spanning the range 0.05 to 2.50 Hz. This frequency range encompasses the wave excitation frequencies and significant modes excited by the unidirectional waves, but excludes large variance low-frequency components. This damage index will take values between 0 and 1, with 0 corresponding to a totally linear system with no energy transfer between modes, and 1 corresponding to a system where all energy at frequencies f_i+f_j is phase coupled to energy at f_i and f_j. Fig. 5 shows the increase in damage index as the single member is progressively damaged (nominal system mass using Seastate 1). Also shown are the results for linear reduced stiffness models. For these cases the individual member stiffness was reduced, but the system model exhibits the same reduced stiffness for both positive and negative global displacements. The damage index is small and consistent in all linear cases, and provides a noise floor above which the presence of damage could be inferred. In practice the baseline case could be derived from the new structure or, if this is not possible, from a detailed FE model of the structure (this facility exists in many cases for offshore structures).

6.2. Parameter sensitivity study

As for all statistical methods, it is important to understand how the results are affected by varying the parameters used in the calculation of the damage index. Fig. 6 shows the results of repeated simulations using the undamaged system and 30 percent through-cracked member cases (as both linear and bilinear systems). The difference between the 10 simulations is in the random source used to generate the wave excitation spectra. Each case represents results obtained with a different seed for the white noise source. The figure serves to demonstrate the consistency achieved in the estimation of the bicoherence function and damage index.

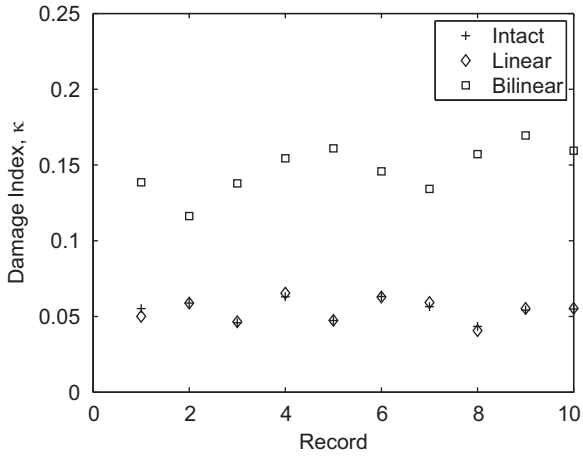

Fig. 6. Damage index calculated for 10 data records using different random sources for wave excitation. Cases for undamaged, 30 percent through-cracked linear, and 30 percent through-cracked bilinear shown.

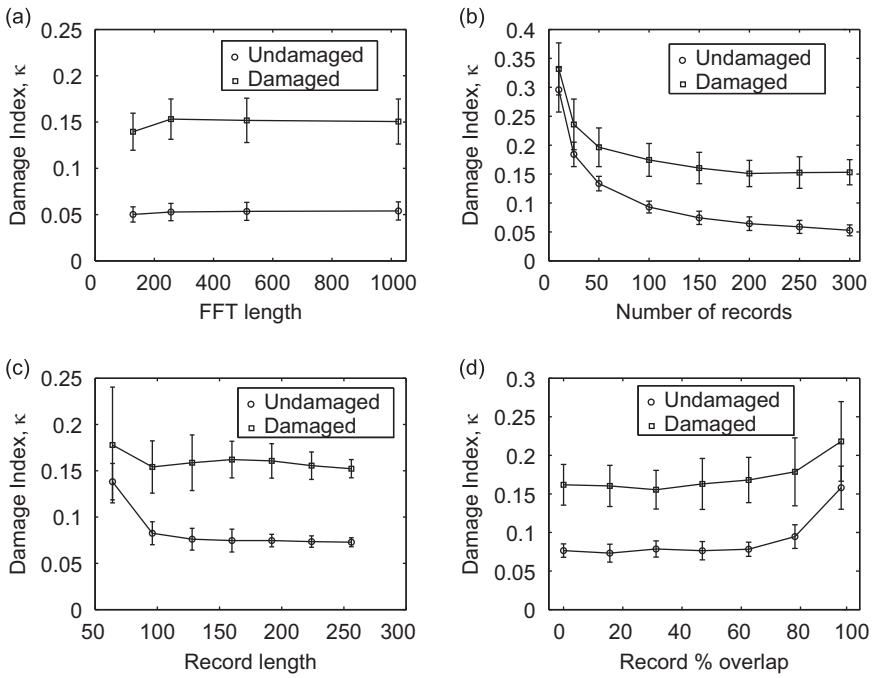

Fig. 7. Sensitivity of damage index value to parameter settings used in its calculation. Undamaged and 30 percent through-cracked cases shown.

Fig. 7 shows results for undamaged and 30 percent through-cracked bilinear systems. Results are presented for the damage index as various parameters used in its calculation are varied. The varied parameters are the length of FFTs used, the number of records used for averaging, the length of individual records, and the percentage overlap between records. These parameters are as described in Section 4.2. The purpose of this figure is to address the issue of parameter sensitivity raised in Section 4.1. In each case, three parameters were fixed while the fourth was varied. Each point is the average value of 10 runs and the error bars are the standard deviation of the results. The following conclusions may be drawn from this study:

- Referring to Fig. 7(a), it can be seen that the values of damage index calculated for the damaged and undamaged cases are consistent and the damaged values are well clear of the noise floor defined by the undamaged values. The FFT length makes little difference to the value of damage index calculated. Using an FFT shorter than 128 results in some inaccuracy, and using FFTs of length greater than 1024 results in substantial increases in computational effort with little benefit.

- Referring to Fig. 7(b), it can be seen that increasing the number of records used results in greater consistency since the calculated curves for damage index flatten with increasing number of records and the error bars reduce. This is due to the larger amount of data used in the calculation. Of course larger amounts of data results in increased computational effort and collection may result in practical difficulties, such as substantial changes in conditions during collection.
- Fig. 7(c) shows that the length of the records used is important, but providing it is greater than 100 samples the damaged case is clearly separated from the noise floor and good consistency is achieved.
- Fig. 7(d) shows that the percent overlap of records has little effect on consistency providing it is kept below 50 percent. Above this value the error bars are seen to increase and the damaged and undamaged values cannot be distinguished.

Values of $M=300$, $N=128$ and $N_{DFT}=256$ were used in all analyses.

6.3. Further results

Fig. 8 demonstrates the necessary insensitivity of the bicoherence-based SHM technique to normal operating variations. Fig. 8(a) shows the increase in damage index with increasing damage levels (a fatigue crack in a single member as before). Three cases are shown: the system with nominal mass, and nominal mass $\times$ 30 percent The structure was excited by Seastate 1 acting in the x-direction. The values for the damage index are consistent in all cases despite the large variations in topside mass.

Fig. 8(b) shows similar results for simulations conducted with nominal mass, excitation using Seastate 1 in the positive x-direction (see Fig. 2) and with different levels of system damping. Three cases are shown: the nominal system (2 percent damping) and also with damping doubled and halved. Again it is seen that the damage index values are consistent in all cases.

Fig. 8(c) shows the variation in damage index under structural excitation by the two seastates described in Section 3. Although such close agreement in the damage indices for the two cases is not seen here, there is clearly a similar trend with increasing damage levels and a significant difference in both cases when compared with the undamaged case and linear systems. This is also seen in Fig. 8(d), which shows the results achieved with the nominal system subject to Seastate 1 but with the action of the waves applied in different directions. The angles relate to the incident angle of the waves upon the structure, with 0° being in the positive x-direction and 90° being in the positive y-direction. The action of the simulated crack is in the x-direction, so when the wave loads are applied perpendicular to the crack (the 90° case) there is very low amplitude motion in the x-direction activating the crack. Despite this, the nonlinear effect is still seen to result in similar values for the damage index.

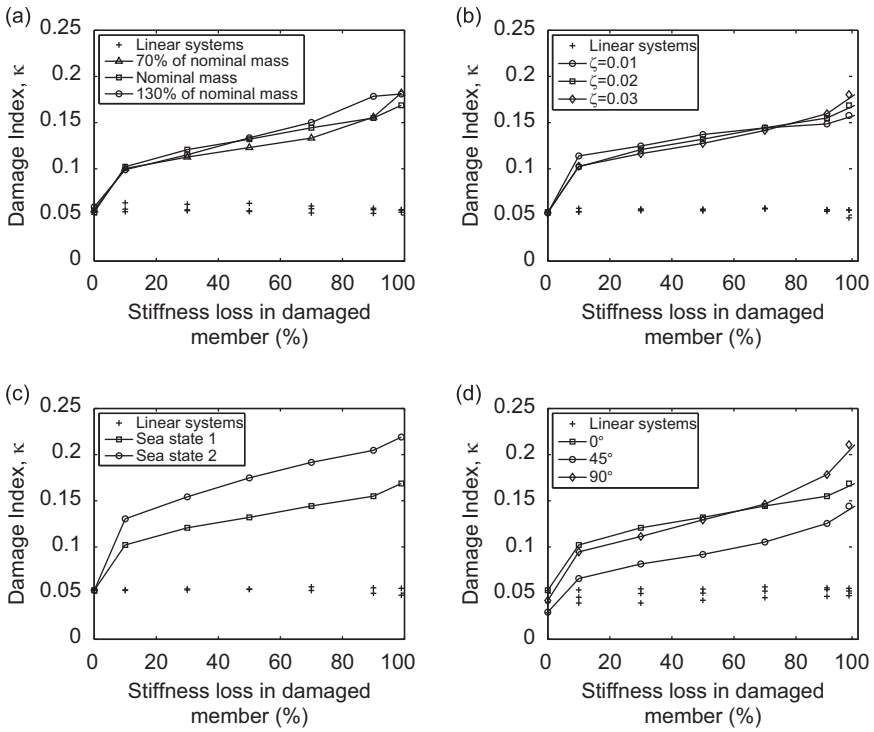

Fig. 8. Damage index for system variations. (a) Mass variation. (b) Damping variation. (c) Different seastates. (d) Different wave load directions.

All the results demonstrate that a positive discrimination could be achieved between damaged and undamaged states, even for very low damage levels (the single damaged member with 10 percent stiffness reduction in this structure corresponds to approximately a 3 percent change in global stiffness at the first structural vibration mode). All results also indicate an increase in the value of damage index for increasing levels of damage, suggesting the possibility of using this technique to also track the progression of damage.

7. Conclusions

A novel SHM technique based upon bicoherence analysis has been applied to a simulated offshore platform. The technique requires no external excitation other than the natural environmental loading that is always present. The technique has been shown to be sufficiently sensitive to detect a 10 percent through-crack in a single member of a complex truss structure. It has also been shown to be robust to large variations in physical parameters and excitation levels that would be seen in the field and which would render many other SHM techniques ineffective. As such this method could provide a robust and sensitive means for early detection and tracking of fatigue damage in such structures at an early stage, in turn improving safety and reducing operating costs through aiding the scheduling of maintenance.

The simulation model is readily extendible to include loading from other sources such as wind and process equipment, and to explore the effect of damage at different locations. Future work will include experimental validation of the technique and extension to locate and quantify the level of damage present in the structure.

References

[1] K. Worden, A.D. Ball, G.R. Tomlinson, Fault location in a framework structure using neural networks, *Smart Mater. Struct.* 2 (1993) 189–200.
[2] I.U. Solodov, Ultrasonics of non-linear contacts: propagation, reflection and NDE application, *Ultrasonics* 36 (1998) 383–390.
[3] V.V. Kazakov, A. Sutin, P.A. Johnson, Sensitive imaging of an elastic nonlinear wavescattering source in a solid, *Appl. Phys. Lett.* 81 (2002) 646–648.
[4] M. Morbidini, P. Duffour, P. Cawley, Vibro-acoustic modulation NDE technique. Part 2: experimental study, *Rev. Prog. Quant. NDE* 24 (2005) 616–623.
[5] D.J. Ewins, *Modal Testing: Theory and Practice*, Research Studies Press, Baldock, UK, 1984.
[6] R. Brincker, P. Kirkegaard, P. Andersen, Damage detection in an offshore structure, *Proceedings of the 13th International Modal Analysis Conference*, 1995, pp. 661–667.
[7] N. Stubbs, S. Park, C. Sikorsky, S. Choi, A global non-destructive damage assessment methodology for civil engineering structures, *Int. J. Syst. Sci.* 31 (11) (2000) 1361–1373.
[8] A. Pandey, M. Biswas, M. Samman, Damage detection from changes in curvature mode, *Journal of Sound and Vibration* 145 (2) (1991) 321–332.
[9] D. Bernal, Flexibility-based damage localization from stochastic realization results, *ASCE J. Eng. Mech.* 132 (6) (2006) 651–658.
[10] A. Dimarogonas, Vibration of cracked structures: a state of the art review, *Eng. Fract. Mech.* 55 (1996) 831–857.
[11] A. Rivola, P.R. White, Bispectral analysis of the bilinear oscillator with application to the detection of fatigue cracks, *J. Sound Vib.* 216 (1998) 889–910.
[12] J.W.A. Fackrell, P.R. White, J.K. Hammond, R.J. Pinnington, The interpretation of the bispectra of vibration signals-ii. Experimental results and applications, *Mech. Syst. Signal Process.* 9 (1995) 267–274.
[13] J.R. Stack, R.G. Harley, T.G. Habetler, An amplitude modulation detector for fault diagnosis in rolling element bearings, *IEEE Trans. Ind. Electron.* Soc. 1–4 (2002) 3377–3382.
[14] J. Nichols, C. Olson, Optimal bispectral detection of weak, quadratic nonlinearities in structural systems, *J. Sound Vib.* 329 (2010) 1165–1176.
[15] Y. Xiang, S.K. Tso, Detection and classification of flaws in concrete structure using bispectra and neural networks, *NDT&E Int.* 35 (2002) 19–27.
[16] J. Chen, I. Hagiwara, X. Su, Q.Z. Shi, A bispectrum feature extraction enhanced structure damage detection approach, *JSME Int. J. Ser. CMech. Syst. Mach. Elem. Manuf.* 45 (2002) 121–126.
[17] D.M. Yang, A.F. Stronach, P. MacConnell, J. Penman, Third-order spectral techniques for the diagnosis of motor bearing condition using artificial neural networks, *Mech. Syst. Signal Process.* 16 (2002) 391–411.
[18] D. Tilley, P. Keogh, K. Mutch, M. Robotham, P. Curran, S. Mehrkar-Asl, Making the eye blink—modelling the operation of the gateshead millennium bridge, *Proc. IMechE Part C—J. Mech. Eng. Sci.* 217 (7) (2003) 735–758.
[19] K. Hasselmann, T. Barnett, E. Bouws, H. Carlson, D. Cartwright, K. Enke, J. Ewing, H. Gienapp, D. Hasselmann, P. Kruseman, A. Meerburg, P. Mller, D. Olbers, K. Richter, W. Sell, H. Walden, Measurements of wind-wave growth and swell decay during the joint north sea wave project (JONSWAP), *Ergnzungsheft Dtsch. Hydrographischen Z. Reihe* 8 (1973) 95.
[20] J. Morison, M.O. Brien, J. Johnson, S. Schaff, Forces exerted by surface waves on piles, *Petro. Trans. Am. Inst. Min. Eng.* 189 (1950) 149–154.
[21] A. Adams, N. Barltrop, *Dynamics of Fixed Marine Structures*, Butterworth-Heinemann Ltd, Oxford, 1950.
[22] A. Hillis, Active motion control of fixed offshore platforms using an extended state observer, *Proc. Inst. Mech. Eng. Part I—J. Syst. Control Eng.* 224 (2010) 53–63.
[23] Y.C. Kim, E.J. Powers, Digital bispectral analysis and its applications to non-linear wave interactions, *IEEE Trans. Plasma Sci.* 7 (2) (1979) 120–131.
[24] J.M. Mendel, Tutorial on higher-order statistics (spectra) in signal-processing and system-theory—theoretical results and some applications, *Proc. IEEE* 79 (3) (1991) 278–305.
[25] P.L. Brockett, M. Hinich, G.R. Wilson, Nonlinear and non-Gaussian ocean noise, *J. Acoust. Soc. Am.* 82 (4) (1987) 1386–1394.
[26] K. Hasselmann, W. Munk, G. Macdonald, Bispectra of ocean waves, in: M. Rosenblatt (Ed.), *Proceedings of the Symposium on Time Series Analysis*, 1963.
[27] C.H. McComas, M.G. Briscoe, Bispectra of internal waves, *J. Fluid Mech.* 97 (March) (1980) 205–213.
[28] S. Elgar, R.T. Guza, Statistics of bicoherence, *IEEE Trans. Acoust. Speech Signal Process.* 36 (10) (1988) 1667–1668.
[29] T.H.C. Herbers, R.T. Guza, Wind-wave nonlinearity observed at the sea-floor. Part II: wave-numbers and 3rd-order statistics, *J. Phys. Oceanogr.* 22 (5) (1992) 489–504.
[30] I.R. Young, Y. Eldeberky, Observations of triad coupling of finite depth wind waves, *Coastal Eng.* 33 (2–3) (1998) 137–154.
[31] M.J. Hinich, M. Wolinsky, Normalizing bispectra, *J. Stat. Plann. Inference* 130 (1–2) (2005) 405–411.
[32] S. Elgar, R.T. Guza, Observations of bispectra of shoaling surface gravity-waves, *J. Fluid Mech.* 161 (1985) 425–448.
[33] S. Elgar, R.T. Guza, Nonlinear model predictions of bispectra of shoaling surface gravity-waves, *J. Fluid Mech.* 167 (1986) 1–18.